Inorganic Chemistry

Article

pubs.acs.org/IC

Amphiphilic Pentaazamacrocyclic Manganese Superoxide Dismutase Mimetics

Dominik Lieb, Isabell Kenkell, Jan Lj. Miljković, Daniel Moldenhauer, Nadine Weber, Milos R. Filipović, Franziska Gröhn, and Ivana Ivanović-Burmazović*

Department of Chemistry and Pharmacy, University of Erlangen-Nürnberg, Egerlandstr. 1, 91058 Erlangen, Germany.

Supporting Information

ABSTRACT: Five newly functionalized pentaazamacrocyclic manganese complexes, with variable lengths and amounts of the aliphatic groups (three compounds with one linear chain containing 12, 16, and 22 carbon atoms, i.e., Mn**L1**, Mn**L2**, and Mn**L3**, respectively, as well as two compounds containing two C12 and C16 chains, Mn**L4** and Mn**L5**, respectively) that are derivatives of the known SOD mimetic, Mn(Me_2-Pyane), have been synthesized. These amphiphilic complexes were characterized by the ESI mass spectrometry, potentiometric titrations, light scattering, cyclic voltammetry, and direct stopped-flow determination of their SOD activity at pH 8.1 and 7.4 (in phosphate and HEPES buffers). The formation of supramolecular aggregates that predominantly exist in the solution as a defined micellar/nanostructure assembly, with an average 400 nm size, has been demonstrated for Mn**L1**. The biological effects of the selected complexes (Mn**L1** and Mn**L2**) on the superoxide level in cytosol and mitochondria have been tested, as well as their effects on the prevention of the lipid peroxidation induced by paraquat. Advantages and disadvantages of the lipophilic pentaazamacrocyclic manganese SOD mimetics in comparison to the corresponding nonsubstituted SOD active complex have been discussed.

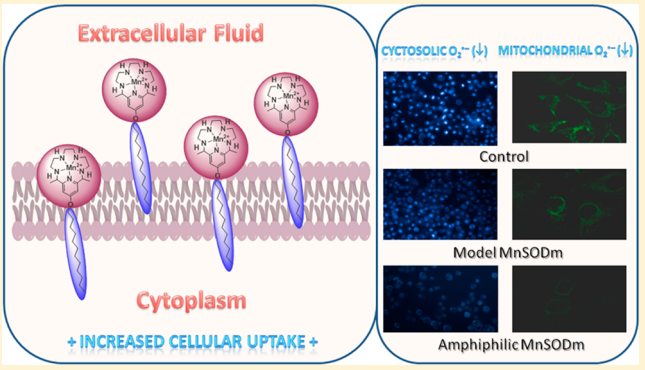

INTRODUCTION

Research on combining metal centers with organic lipophilic ligand frameworks containing elongated aliphatic carbon chains is expanding due to a widespread field of potential applications for such compounds, including the medical area (e.g., magnetic resonance imaging (MRI) contrast agents (CAs)),[1,2] material sciences (liquid crystals based on metallomesogens),[3] and the field of catalysis.[4] In that context, manganese complexes are designed and tested for medical applications, ranging from superoxide-dismutase mimetics (SODm)[5,6] to MRI contrast agents.[7−9] Designing suitable ligand frameworks that assist in the formation of reactive (kinetically labile) and thermodynamically stable metal complexes, with required compartmentalization in targeted cells and tissues, is one of the most important tasks to be considered when trying to use such metal complexes in the aforementioned areas. For both mentioned applications (SODm and MRI contrast agents), the lability of the bound water molecules is crucial. It enables efficient binding of superoxide required for an inner-sphere electron transfer that is a predominant mechanism operating in the SOD catalysis.[10] On another hand, the fast water exchange results in an enhancement of the NMR proton signal.[11] Further requirements are a sufficiently high lipophilicity for cell membrane penetration and an ample water solubility to accumulate in physiologically beneficial concentrations at the desired location. The ability of having both lipophilic and hydrophilic characteristics—amphiphilicity—enables compounds of such structural composition to form micellar structures, which have been studied, for example, as potential vehicles for drug delivery into various tissues.[12,13] The formation of micelles can also be beneficial for the design of MRI contrast agents due to an increased local concentration of labile water molecules combined with a decreased molecular motion of the enlarged aggregates that both decrease the T_1 parameter (longitudinal relaxation time of the electron-spin on exchanging water molecules).[2,11,14]

Although SOD active metal-based compounds with increased lipophilicity are known in the literature,[15−17] the concept of introducing a long linear aliphatic chain into the ligand framework of the manganese pentaazamacrocyclic SOD mimetics, with the potential of forming micellar structures, has not been reported yet. This class of manganese complexes is known for its prominent SOD activity and putative selectivity toward superoxide.[5a,18] Although it was reported that they do not react with nitric oxide, hydrogen peroxide, and peroxynitrite,[5a,18] more recent studies demonstrated their ability to catalytically react with NO and generate nitroxyl (HNO).[10,19] Thus, the true nature of the reactions behind their biological

Received: September 30, 2013
Published: December 26, 2013

   dx.doi.org/10.1021/ic402469t | *Inorg. Chem.* 2014, 53, 1009−1020

Chart 1. Organic Frameworks L1−L5 for a New Class of Lipohilic Manganese(II) SOD Mimetics Reported in This Work with Varying Lengths and Amounts of Aliphatic Side Chains As Well As Structures of Known SOD Mimetics Mn(Me_2-Pyane) and M40403

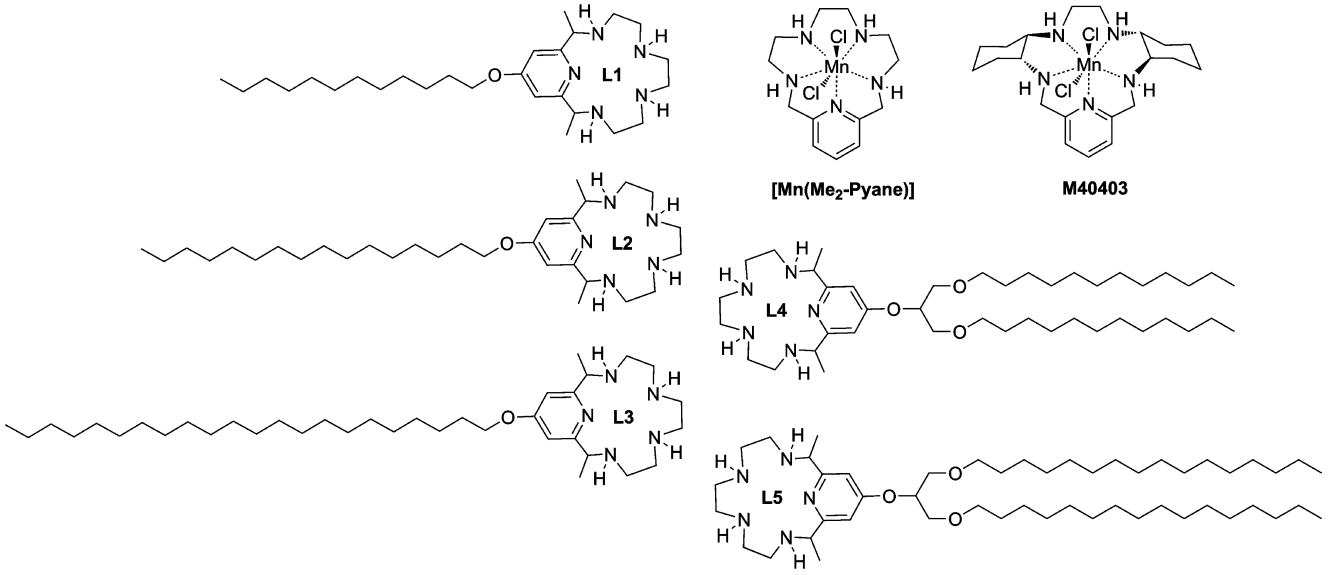

effects is still unrevealed, and its elucidation represents a challenging research topic.

In this work, our aim was to extend the library of Mn complexes that belong to this class of well established SOD mimetics, by synthesizing the amphiphilic analogues of Mn(Me_2-Pyane), a proven SOD active complex.[20−22] The two structural motives, elongated hydrocarbon chain(s) and a macrocyclic core, are linked by an ether functionality resulting in a class of new ligand frameworks, **L1−L5**, for the binding of manganese(II), as shown in Chart 1. The solution behavior and reactivity of synthesized manganese complexes has been studied by determining their acid−base and redox properties, their ability to form supramolecular aggregates, and their *in vitro* catalytic activity toward superoxide decomposition. In addition, cell culture studies have been performed to evaluate an effect of the increased lipophilicity of some of these complexes on their biological effects.

EXPERIMENTAL SECTION

Materials and Methods. All reactions were performed under an argon atmosphere. Reagents and solvents which are commercially available were purchased from Sigma Aldrich, were of *p.a.* grade, and were used without further purification. Only anhydrous solvents (purchased from Sigma Aldrich or Acros Organics) were used for syntheses. Deionized Millipore water was used for all measurements. Carlo Erba Elemental Analyzers 1106/1108 and a Bruker Avance DPX 300 NMR spectrometer were used for elemental and NMR analyses, respectively. IR spectra were recorded as KBr pellets on a Mattson FT-IR 60 AR. Column chromatography was performed with silica gel 60 (high-purity grade, pore size 60 Å, 70−230 mesh, 63−200 μm) purchased from Sigma Aldrich. Thin layer chromatography was performed with TLC silica gel 60 F_{254} precoated plastic and aluminum sheets purchased from Merck.

Synthesis of 4-Chloro-2,6-diacetylpyridine, 1..[23,24] 4-Chloropyridine hydrochloride (23.75 g, 15.84 mmol) was dissolved in water, and the acidic yellow solution was basified with saturated sodium carbonate solution. This solution was extracted with dichloromethane (DCM; 3 × 100 mL), and the combined organic fractions were dried with $MgSO_4$. After evaporation of the solvent, 4-chloropyridine was obtained as a yellow oil in 95% yield and was used without further characterization. To 1 L of a 0.4 M H_2SO_4 solution, the freshly prepared 4-chloropyridine was added while stirring. Pyruvic acid (27.50 g, 21.70 mL, 313.00 mmol) and an aqueous solution of silver nitrate (1.50 g, 8.83 mmol; dissolved in 3.00 mL water) were additionally added. $(NH_4)_2S_2O_8$ (110.00 g, 438.00 mmol) was added while stirring, followed by the evolution of carbon dioxide. The solution was stirred at RT overnight, and the precipitate was filtered off and washed with DCM. The remaining solution was combined with a DCM wash of the precipitate and was extracted with DCM (3 × 200 mL). The combined organic residues were dried with $MgSO_4$. After evaporation of the solvent, crude **1** was obtained as an orange oil and purified *via* column chromatography (SiO_2, Hep/EtOAc; 5/1). Compound **1** (7.80 g, 25%) was obtained as a white powder. Anal. Calcd for $C_9H_8ClNO_2$: C, 54.70; H, 4.08; N, 7.09. Found: C, 54.13; H, 3.93; N, 6.92. ^{1}H NMR (300 MHz, $CDCl_3$, 25 °C): δ [ppm] 2.78 (s, 6H, C(O)C$\underline{H}_3$), 8.18 (s, 2H, Ar$\underline{H}$). ^{13}C NMR (75 MHz, $CDCl_3$, 25 °C): δ [ppm] 25.41, 124.70, 146.69, 153.70, 197.89.

Synthesis of 4-Chloro-2,6-bis[2-methyl-(1,3-dioxolan-2-yl)]-pyridine, 2.[25] To a solution of **1** (6.85 g, 34.70 mmol) in 300 mL toluene, *p*-toluenesulfonic acid (0.38 g, 2.21 mmol) and 1,2-ethyleneglycol (31.70 g, 28.50 mL, 510.00 mmol) were added. The reaction mixture was refluxed for 24 h, and water was removed *via* a Dean−Stark water separator. After cooling to RT, the solvent was removed *in vacuo*. The resulting yellow oil was dissolved in 150 mL DCM and washed with 100 mL of a 5% $NaHCO_3$-solution in water. The aqueous wash was extracted one more time with 150 mL of DCM. The combined organic solutions were dried with $MgSO_4$, and the DCM was removed afterward. The obtained yellow oil was purified *via* a short silica column ($CHCl_3$/EtOAc; 5/2). The product was obtained as a colorless oil, which solidified in the refrigerator (9.41 g, 95%). ^{1}H NMR (300 MHz, $CDCl_3$, 25 °C): δ [ppm] 1.74 (s, 6H, C(O)C$\underline{H}_3$), 3.93 (m, 4H, $CH_2C\underline{H}_2$), 4.09 (m, 4H, $C\underline{H}_2H_2$), 7.49 (s, 2H, Ar$\underline{H}$). ^{13}C NMR (75 MHz, $CDCl_3$, 25 °C): δ [ppm] 24.58, 65.13, 108.34, 119.17, 145.01, 162.28.

General Procedure for the Synthesis of 4-Alkoxy-2,6-diacetyl Ketals, 3a−3e.[26] To a solution of compound **2** (3.00 g, 10.5 mmol) in 40 mL of DMSO, NaOH (2.0 g, 50.0 mmol) was added while stirring followed by a color change from yellow to deep orange. To this solution, the respective alcohol (10.5 mmol) was slowly added, and the resulting mixture was heated to 110 °C for 24 h. After cooling to RT, the deep dark-brown solution was added to a 200 mL ice−water mixture resulting in a brown suspension. The aqueous solution was extracted with diethylether (Et_2O; 3 × 100 mL), and the combined organic extracts were washed with 200 mL of brine solution

dx.doi.org/10.1021/ic402469t | Inorg. Chem. 2014, 53, 1009−1020

and dried with $MgSO_4$. After filtration and removal of the solvent, the crude product was obtained as orange oil. Compounds **3a**–**3c** were used without further purification, and **3d** and **3f** were purified *via* column chromatography (SiO_2, $CHCl_3$/EtOAc; 5/2). 1,3-Bis-(dodecyloxy)propan-2-ol and 1,3-bis(hexadecyl-oxy)propan-2-ol were obtained using a published procedure.[27]

4-Dodecyloxy-2,6-bis[2-methyl-(1,3-dioxolan-2-yl)]pyridine, ***3a***. Yield: 3.29 g, 72%. ^{1}H NMR (300 MHz, $CDCl_3$, 25 °C): δ 0.88 (m, 3H, $CH_2C\underline{H}_3$), 1.27 (s, 16H, aliphat. $\underline{H}$), 1.31 (m, 2H, aliphat. H), 1.74 (s, 6H, $C\underline{H}_3CO_2$), 1.78 (m, 2H, aliphat. $\underline{H}$), 3.92 (m, 4H, $OC\underline{H}_2CH_2O$), 4.01 (t, $^3J_{H,H}$ = 6.6, 2H, $C\underline{H}_2CH_2$), 4.08 (m, 4H, $OC\underline{H}_2CH_2O$), 6.99 (s, 2H, Ar$\underline{H}$). ^{13}C NMR (75 MHz, $CDCl_3$, 25 °C): δ [ppm] 14.10, 22.66, 24.73, 25.96, 29.33, 29.63, 32.82, 64.95, 68.07, 105.02, 108.66, 162.25, 166.31.

4-Hexadecyloxy-2,6-bis[2-methyl-(1,3-dioxolan-2-yl)]pyridine, ***3b***. Yield: 3.35 g, 65%. ^{1}H NMR (300 MHz, $CDCl_3$, 25 °C): δ 0.87 (m, 3H, $CH_2C\underline{H}_3$), 1.27 (m, 24H, aliphat. $\underline{H}$), 1.31 (m, 2H, aliphat. $\underline{H}$), 1.73 (s, 6H, $C\underline{H}_3CO_2$), 1.76 (m, 2H, aliphat. $\underline{H}$), 3.93 (m, 4H, $OC\underline{H}_2CH_2O$), 4.00 (t, $^3J_{H,H}$ = 6.6 Hz, 2H, $ArOC\underline{H}_2CH_2$), 4.08 (m, 4H, $OC\underline{H}_2CH_2O$), 7.00 (s, 2H, Ar$\underline{H}$); see Figure S1. ^{13}C NMR (75 MHz, $CDCl_3$, 25 °C): δ [ppm] 14.11, 22.68, 24.73, 25.96, 29.34, 29.58, 29.63, 31.92, 64.95, 68.07, 105.04, 108.67, 162.24, 166.31; see Figure S1.

4-Docosanoxy-2,6-bis[2-methyl-(1,3-dioxolan-2-yl)]pyridine, ***3c***. Yield: 3.08 g, 51%. ^{1}H NMR (300 MHz, $CDCl_3$, 25 °C): δ 0.87 (m, 3H, $CH_2C\underline{H}_3$), 1.25 (m, 38H, aliphat. $\underline{H}$), 1.74 (s, 6H, $C\underline{H}_3CO_2$), 1.77 (m, 2H, aliphat. $\underline{H}$), 3.93 (m, 4H, $OC\underline{H}_2CH_2O$), 4.01 (t, $^3J_{H,H}$ = 6.6 Hz, 2H, $C\underline{H}_2CH_2$), 4.08 (m, 4H, $OC\underline{H}_2CH_2O$), 6.98 (s, 2H, Ar$\underline{H}$). ^{13}C NMR (75 MHz, $CDCl_3$, 25 °C): δ [ppm] 14.10, 22.66, 24.75, 24.77, 25.74, 25.81, 25.88, 26.23, 28.97, 29.30, 29.58, 29.61, 31.90, 32.81, 64.95, 68.08, 105.00, 108.66, 162.24, 166.30.

4-{1,3-Bis[(dodecyloxy)propan-2-oxy]-2,6-bis[2-methyl-(1,3-dioxolan-2-yl)]}pyridine, ***3d***. Yield: 2.55 g, 55%. Off-white solid after purification (R_f = 0.65). Anal. Calcd for $C_{40}H_{71}NO_7$: C, 70.86; H, 10.56; N, 2.07. Found: C, 71.11; H, 10.15; N, 1.77. ^{1}H NMR (300 MHz, $CDCl_3$, 25 °C): δ [ppm] 0.88 (m, 6H, $CH_2C\underline{H}_3$), 1.26 (s, 36H, aliphat. $\underline{H}$), 1.56 (m, 4H, $OCH_2C\underline{H}_2CH_2$), 1.73 (s, 6H, $C\underline{H}_3CO_2$), 3.44 (m, 4H, $CHCH_2OC\underline{H}_2$), 3.67 (m, 4H, $CHC\underline{H}_2OCH_2$), 3.91 (m, 4H, $OCH_2C\underline{H}_2O$), 4.11 (m, 4H, $OC\underline{H}_2CH_2O$), 4.66 (m, 1H, $ArOC\underline{H}(CH_2OCH_2)_2$), 7.10 (s, 2H, Ar$\underline{H}$). ^{13}C NMR (75 MHz, $CDCl_3$, 25 °C): δ [ppm] 14.10, 21.03, 24.72, 29.36, 29.47, 29.69, 31.92, 60.37, 64.95, 69.72, 71.93, 106.09, 108.63, 162.28, 165.70.

4-{1,3-Bis[(hexadecyloxy)propan-2-oxy]-2,6-bis[2-methyl-(1,3-dioxolan-2-yl)]}pyridine, ***3e***. Yield: 3.51 g, 60%. Off-white solid after purification (R_f = 0.61). Anal. Calcd for $C_{48}H_{87}NO_7$: C, 72.96; H, 11.10; N, 1.77. Found: C, 75.91; H, 13.15; N, 1.37. ^{1}H NMR (300 MHz, $CDCl_3$, 25 °C): δ [ppm] 0.87 (m, 6H, $CH_2CH_2C\underline{H}_3$), 1.25 (s, 56H, aliphat. $\underline{H}$), 1.55 (m, 4H, $OCH_2C\underline{H}_2CH_2$), 1.73 (s, 6H, $C\underline{H}_3CO_2$), 3.45 (m, 4H, $ArOCH(CH_2OC\underline{H}_2)_2$), 3.65 (m, 4H, $ArOCH(C\underline{H}_2OCH_2)_2$), 3.91 (m, 4H, $OCH_2C\underline{H}_2O$), 4.06 (m, 4H, $OC\underline{H}_2CH_2O$), 4.67 (m, 1H, $ArOC\underline{H}(CH_2O)_2$), 7.08 (s, 2H, Ar$\underline{H}$); see Figure S2. ^{13}C NMR (75 MHz, $CDCl_3$): δ [ppm] 14.09, 21.01, 22.66, 24.70, 26.04, 29.34, 29.45, 29.68, 31.90, 60.36, 64.93, 69.70, 71.91, 106.07, 108.61, 162.26, 165.68; see Figure S2.

General Procedure for the Synthesis of 4-Alkoxy-2,6-diacetyl pyridines, 4a–4c.[28] To a solution of HBr (48%, 35 mL) and $(Bu_4N)Br$ (0.17 g, 0.53 mmol), the respective 4-alkoxy-2,6-bis[2-methyl-(1,3-dioxolan-2-yl)]pyridine **3a**–**3c** (5.25 mmol) was added, and the resulting mixture was refluxed for 3 h at 100 °C. The color of solution turned from deep orange to dark brown during the course of the reaction. After cooling to RT, the reaction solution was added dropwise to 75 mL of a stirred saturated Na_2CO_3-solution, accompanied by a precipitation of brown solid. The resulting mixture was slightly alkalized with saturated $NaHCO_3$ solution and extracted with DCM (3 × 100 mL). The combined organic phases were successively washed with 400 mL of water and 400 mL of brine solution and subsequently dried with $MgSO_4$. The obtained brown solid was purified *via* column chromatography (SiO_2, $CHCl_3$/EtOAc; 5/2); the respective product was obtained as off-white powder.

4-Dodecyloxy-2,6-diacetylpyridine, ***4a***. Yield: 1.79 g, 98%. Off-white solid after purification (R_f = 0.71). Anal. Calcd for $C_{21}H_{33}NO_3$: C, 72.58; H, 9.57; N, 4.03. Found: C, 70.16; H, 10.22; N, 4.06. ^{1}H NMR (300 MHz, $CDCl_3$, 25 °C): δ [ppm] 0.87 (m, 3H, $CH_2CH_2C\underline{H}_3$), 1.26 (s, 16H, aliphat. $\underline{H}$), 1.44 (m, 2H, aliphat. $\underline{H}$), 1.81 (m, 2H, $OCH_2C\underline{H}_2CH_2$), 2.76 (s, 6H, $C\underline{H}_3C(O)$), 4.10 (m, 2H, $ArOC\underline{H}_2CH_2$), 7.68 (s, 2H, Ar$\underline{H}$). ^{13}C NMR (75 MHz, $CDCl_3$, 25 °C): δ [ppm] 14.14, 22.65, 25.75, 25.82, 29.24, 29.55, 29.62, 31.99, 68.92, 110.96, 154.54, 167.05, 199.53.

4-Hexadecyloxy-2,6-diacetylpyridine, ***4b***. Yield: 1.91 g, 90%. Off-white solid after purification (R_f = 0.7). Anal. Calcd for $C_{25}H_{41}NO_3$: C, 74.40; H, 10.24; N, 3.47. Found: C, 72.67; H, 9.99; N, 3.86. ^{1}H NMR (300 MHz, $CDCl_3$, 25 °C): δ [ppm] 0.88 (m, 3H, $CH_2CH_2C\underline{H}_3$), 1.26 (s, 24H, aliphat. $\underline{H}$), 1.42 (m, 2H, aliphat. $\underline{H}$), 1.81 (m, 2H, $OCH_2C\underline{H}_2CH_2$), 2.76 (s, 6H, $C\underline{H}_3C(O)$), 4.10 (m, 2H, $ArOC\underline{H}_2CH_2$), 7.68 (s, 2H, Ar$\underline{H}$); see Figure S3. ^{13}C NMR (75 MHz, $CDCl_3$, 25 °C): δ [ppm] 14.11, 22.69, 25.71, 25.82, 28.75, 29.24, 29.34, 29.51, 29.55, 29.62, 31.91, 68.91, 110.92, 154.54, 167.05, 199.57; see Figure S3.

4-Docosanoxy-2,6-diacetylpyridine, ***4c***. Yield: 2.0 g, 78%. Off-white solid after purification (R_f = 0.6). Anal. Calcd for $C_{31}H_{53}NO_3$: C, 76.34; H, 10.95; N, 2.87. Found: C, 76.00; H, 10.21; N, 3.16. ^{1}H NMR (300 MHz, $CDCl_3$, 25 °C): δ [ppm] 0.88 (m, 3H, $CH_2CH_2C\underline{H}_3$), 1.25 (s, 36H, aliphat. $\underline{H}$), 1.43 (m, 2H, aliphat. $\underline{H}$), 1.81 (m, 2H, $OCH_2C\underline{H}_2CH_2$), 2.76 (s, 6H, $C\underline{H}_3C(O)$), 4.11 (m, 2H, $ArOC\underline{H}_2CH_2$), 7.68 (s, 2H, Ar$\underline{H}$). ^{13}C NMR (75 MHz, $CDCl_3$, 25 °C): δ [ppm] 14.15, 22.69, 25.73, 25.82, 26.03, 28.79, 29.26, 29.52, 29.54, 29.62, 32.00, 68.90, 110.91, 154.55, 167.02, 199.59.

General Procedure for the Synthesis of 4-Alkoxy-2,6-diacetyl Pyridines, 4d and 4e. The respective 4-(1,3-bis(alkoxy)-propan-2-oxy)pyridine ketal (1.26 mmol) was dissolved in 50 mL of THF, and 2 mL of conc. $HClO_4$ was added dropwise. The solution was refluxed for 2 h and cooled down to RT. Saturated $NaHCO_3$ solution was added dropwise until neutral pH, and the aqueous solution was extracted with Et_2O (3 × 50 mL). The organic fractions were combined and dried ($MgSO_4$), and the solvent was removed *in vacuo*. The crude solid was purified with a short silica plug (100% DCM), and the appropriate 4-(1,3-bis(alkoxy)prop-2-oxy)-2,6-dicacetylpyridine was obtained as off-white powder.

Synthesis of 4-[1,3-Bis(dodecyloxy)propan-2-oxy]-2,6-diacetylpyridine, ***4d***. Yield: 2.85 g, 92%. Anal. Calcd for $C_{36}H_{63}NO_5$: C, 73.30; H, 10.76; N, 2.37. Found: C, 73.27; H, 10.94; N, 2.08. ^{1}H NMR (300 MHz, $CDCl_3$, 25 °C): δ [ppm] 0.88 (m, 6H, $CH_2CH_2C\underline{H}_3$), 1.25 (s, 36H, aliphat. $\underline{H}$), 1.50 (m, 4H, $OCH_2C\underline{H}_2CH_2$), 2.77 (s, 6H, $C\underline{H}_3C(O)$), 3.40 (m, 4H, $ArOCH(CH_2OC\underline{H}_2)_2$), 3.63 (m, 4H, $ArOCH(C\underline{H}_2OCH_2)_2$), 4.82 (m, 1H, $ArOC\underline{H}(CH_2O)_2$), 7.80 (s, 2H, Ar$\underline{H}$). ^{13}C NMR (75 MHz, $CDCl_3$): δ [ppm] 14.12, 22.71, 25.64, 29.38, 29.42, 29.51, 29.63, 31.90, 69.87, 71.90, 112.10, 154.55, 166.79, 199.31.

Synthesis of 4-[1,3-Bis(hexadecyloxy)propan-2-oxy]-2,6-diacetylpyridine, ***4e***. Yield: 3.24 g, 88%. Anal. Calcd for $C_{44}H_{79}NO_5$: C, 75.27; H, 11.34; N, 1.99. Found: C, 75.60; H, 11.79; N, 1.76. ^{1}H NMR (300 MHz, $CDCl_3$, 25 °C): δ [ppm] 0.88 (m, 6H, $CH_2CH_2C\underline{H}_3$), 1.26 (s, 52H, aliphat. $\underline{H}$), 1.51 (m, 4H, $OCH_2C\underline{H}_2CH_2$), 2.75 (s, 6H, $C\underline{H}_3C(O)$), 3.42 (m, 4H, $ArOCH(CH_2OC\underline{H}_2)_2$), 3.66 (m, 4H, $ArOCH(C\underline{H}_2OCH_2)_2$), 4.79 (m, 1H, $ArOC\underline{H}(CH_2O)_2$), 7.79 (s, 2H, Ar$\underline{H}$); see Figure S4. ^{13}C NMR (75 MHz, $CDCl_3$): δ [ppm] 14.11, 22.69, 25.69, 26.03, 29.36, 29.43, 29.54, 29.62, 29.70, 31.92, 69.85, 71.91, 112.00, 154.53, 166.76, 199.34; see Figure S4.

General Procedure for the Synthesis of the Mn(II) Complexes, MnL1–MnL5.[29] $MnCl_2$ (0.18 g, 1.43 mmol) was dissolved in 30 mL of EtOH, and triethylenetetraamine (0.21 g, 1.43 mmol) was added while stirring. The pale orange solution was kept at RT for 30 min, and afterward **4** (1.43 mmol) was added. The mixture was refluxed for 5 h, and the color of the solution turned slowly to dark orange. The solution was cooled down to 4 °C. $NaBH_4$ (0.86 g, 23.0 mmol, 16 equiv) was added (six portions in 15 min time intervals), and the resultant mixture was allowed to stir at RT for 18 h. Additional $NaBH_4$ (0.22 g, 5.76 mmol, 4 equiv) was added, and the beige mixture was stirred for 3 h at 55 °C. After cooling down to RT,

dx.doi.org/10.1021/ic402469t | *Inorg. Chem.* 2014, 53, 1009–1020

the solvent was removed, and excess $NaBH_4$ was quenched with 10 mL of 2 M LiCl in MeOH. MeOH was removed *in vacuo*, and brine solution was added to the residue until all solids dissolved. The aqueous solution was extracted with DCM (3 × 50 mL), and the combined organic phases were dried with $MgSO_4$. The complex was purified by column chromatography (SiO_2, DCM/MeOH; 90:10).

*[Mn(**L1**)Cl$_2$]*. Yield: 0.26 g, 30%. Solubility in 60 mM HEPES buffer at pH = 7.4 and 25 °C: 4 mM. Anal. Calcd for [Mn (**L1**)Cl_2]·1/2H_2O·1/2EtOH: C, 54.28; H, 8.95; N, 11.30. Found: C, 54.79, H, 9.34, N, 10.71. IR (KBr): [cm^{-1}] 3334.80 (s), 3249.94 (s), 3189.18 (s), 2921.24 (s), 2851.62 (s), 1604.50 (s), 1568.38 (m), 1448.53 (s), 1379.95 (m), 1343.28 (s), 1303.21 (m), 1134.10 (m), 1025.35 (m), 946.44 (m), 888.48 8 (m), 660.80 (w).

*[Mn(**L2**)Cl$_2$]*. Yield: 0.25 g, 26%. Solubility in 60 mM HEPES buffer at pH = 7.4 and 25 °C: 2 mM. Anal. Calcd for [Mn(**L2**)Cl_2]·1H_2O: C, 56.27; H, 9.29; N, 10.58. Found: C, 56.79; H, 9.44; N, 10.60. IR (KBr): [cm^{-1}] 2920.35 (s), 2850.66 (s), 1605.04 (s), 1569.20 (s), 1455.63 (s), 1378.48 (m), 1342.72 (s), 1301.89 (m), 1258.55 (w), 1136.97 (s), 1062.08 (m), 1026.70 (s), 947.24 (s), 888.56 (s), 816.13 (s).

*[Mn(**L3**)Cl$_2$]*. Yield: 0.35 g, 31%. Solubility in 60 mM HEPES buffer at pH = 7.4 and 25 °C: 0.5 mM. Anal. Calcd for [Mn(**L3**)Cl_2]·4H_2O: C, 55.56; H, 9.95; N, 8.76. Found: C, 55.61; H, 9.63; N, 8.80. IR (KBr): [cm^{-1}] 3248.35 (s), 2919.31 (s), 2850.25 (s), 1605.45 (s), 1570.31 (m), 1455.48 (s), 1340.63 (s), 1137.94 (s), 1034.33 (m), 808.57 (m).

*[Mn(**L4**)Cl$_2$]*. Yield: 0.17 g, 21%. Solubility: nonsoluble in aqueous solutions. Anal. Calcd for [Mn(**L4**)Cl_2]: C, 60.78; H, 9.84; N, 8.44. Found: C, 61.04; H, 9.94; N, 8.02. IR (KBr): [cm^{-1}] 3248.91 (s), 2856.19 (s), 1605.78 (s), 1569.20 (s), 1455.63 (s), 1378.48 (m), 1365.23 (w), 1342.72 (s), 1314.81 (m), 1258.55 (w), 1072.16 (m), 1026.70 (s), 940.37 (s), 886.56 (s).

*[Mn(**L5**)Cl$_2$]*. Yield: 0.44 g, 33%. Solubility: nonsoluble in aqueous solutions. Anal. Calcd for [Mn(**L5**)Cl_2]: C, 63.74; H, 10.38; N, 7.43. Found: C, 64.14; H, 10.91; N, 7.33. IR (KBr): [cm^{-1}] 3197.30 (s), 2858.56 (s), 1607.12 (m), 1598.45 (w), 1569.20 (s), 1455.63 (s), 1378.48 (m), 1342.72 (s), 1301.89 (m), 1258.55 (w), 1136.97 (s), 1062.08 (m), 1026.70 (s), 947.24 (s), 888.56 (s), 816.13 (s).

Electrochemistry. Cyclic voltammetry measurements were performed using an Autolab instrument with a PGSTAT 30 potentiostat. A three-electrode arrangement was employed consisting of a platinum disk working electrode (A = 0.07 cm^2; Metrohm), a platinum auxiliary electrode (Metrohm) and a Ag/AgCl (2 M LiCl in EtOH; Metrohm) reference electrode (0.164 V vs SHE at 21 °C) for the measurements in anhydrous MeOH or DMSO. The measurements in DMSO were performed in the presence of 0.1 M tetrabutylammonium hexafluorophosphate as the supporting electrolyte, and the measurements in MeOH were performed in 0.1 M LiCl solutions. All solutions were degassed with nitrogen (1 min/mL). During the measurements, the nitrogen atmosphere was maintained. The sample concentration was 1.0 mM for each complex, and the experiments were performed at 21 °C.

Electron-Spray-Ionization (ESI) Mass Spectrometry. High mass accuracy ESI spectra were recorded on an ultrahigh-resolution ESI-Time-Of-Flight MS, a Bruker Daltoniks (Bremen, Germany) maXis. Spectra were obtained in positive-ion mode, with the capillary held at 4000 V. The drying gas flow rate was 7.0 L/min with a temperature of 180 and 4 °C for the cryo-spray measurements. The nebulizer gas was at a pressure of 30.5 psi/2 bar. The m/z range detected was from 100 to 2000 for standard (180 °C) and from m/z 500 to 4000 for cryo (−30 °C) measurements. A calibration tune mix (Agilent Technologies) was sprayed immediately prior to analysis in order to assist in the identification of peaks, thus ensuring a very high mass accuracy. The flow rate of the solutions was 300 μL/h. The samples were dissolved in water (Mn**L1**−Mn**L3**) or MeOH (Mn**L4** and Mn**L5**), and the metal complex concentrations were 1 × 10^{-4} M each. Peaks were identified with the aid of the simulated isotopic patterns created within the Bruker DataAnalysis software.

Potentiometric Titrations. Potentiometric measurements were performed on a Metrohm 702 SM Titrino in a jacketed, airtight glass titration cell equipped with a combined pH glass electrode (Metrohm), N_2 inlet and outlet, and a graduated 10 mL microburet (Metrohm). The electrode was filled with 3 M NaCl and was calibrated using three different commercially available standard buffer solutions of pH 4.0, 7.0, and 10.0. A carbonate-free 0.05 M NaOH solution was prepared with nitrogen-saturated deionized Millipore water. The NaOH solution was standardized by titrations with a 0.05 M potassium hydrogen phthalate solution. Gran's method[30] was used to measure carbonate in the NaOH standard solution (carbonate content 0.08%). All solutions were adjusted to an ionic strength of 0.1 M with tetramethylammonium chloride (Me_4NCl) prior to the titrations. The temperature was maintained by circulating thermostatted water through the outer jacket of the cell. All measurements were carried out with a constant atmosphere of nitrogen maintained above the solution. The concentration of complexes was 1.0 mM for each titration. Species distribution calculations and determination of the corresponding protonation equilibrium and stability constants were performed using the computer program TITFIT.[31]

Dynamic and Static Light Scattering. A sample of Mn**L1** with c = 1.72 × 10^{-3} mol L^{-1} (1.0 g L^{-1}) was prepared in Milli-Q ultrapure water (>18.2 MΩ cm^{-1}). The measurement was carried out using a CGS 3 goniometer (ALV Langen, Germany), a HeNe laser with a wavelength of λ = 632.8 nm with 22 mW output power, and an ALV 5000 correlator with 320 channels. A range of scattering angles of 30° ≤ θ ≤ 150° was covered. For dynamic light scattering, the time autocorrelation function of the scattered intensity g2(τ) was measured and converted into the scattered electric field autocorrelation function g1(τ) via Siegert relation. The electric field autocorrelation functions were analyzed by regularized inverse Laplace transformation using the program CONTIN by Provencher. The apparent diffusion coefficient Dapp was calculated from the mean relaxation time using the relation Dapp = q − 2τ − 1. Dapp was extrapolated to zero scattering vector square and D0app and converted to the hydrodynamic radius using the Stokes−Einstein relationship. The quoted hydrodynamic radius thus represents the inverse z-average and the standard deviation of the size. In static light scattering, the average sample, solvent, and standard (toluene) scattering intensity were recorded in dependence on the scattering angle.

Direct Determination of SOD-Activity *via* Stopped-Flow Measurements. The SOD activity of the complexes was determined by using direct rapid-scan UV−vis detection of superoxide decomposition in aqueous media and global analysis of the entire time-resolved spectra. This method required a double mixer stopped-flow system equipped with a high-density mixer for efficient mixing of aqueous buffer solutions, containing the investigated complexes, with a DMSO solution of KO_2 (in a 10:1 volume ratio). This system is combined with a fast diode array detector (0.5 ms integration time) and a laser driven light source. The exact experimental method used for determination of the SOD activity of novel amphiphilic compounds was reported by us previously.[21] In general, the measurements were carried out in 60 mM 4-(2-hydroxyethyl)-1-piperazineethanesulfonic acid buffer (HEPES) at pH 7.4 or 8.1 or a 50 mM phosphate buffer at pH 7.4, respectively. The buffer solutions were treated with chelex 100 chelating resin for at least the complex solutions. Measurements were performed under actual catalytic conditions, with a high excess of superoxide (2.00 × 10^{-4} M) over the complexes that were used in concentrations of 1.13, 2.25, 4.50, and 9.00 × 10^{-7} M.

Cell Treatment. Concentrated stock solutions of Mn complexes (2 mM) were made in PBS and then added to the cell culture medium to achieve desired final concentrations. Into the medium of the control cells, corresponding volumes of PBS were added.

Fluorescent Microscopy. Fluorescent microscopy was carried out using a Carl Zeiss Axiovert 40 CFL inverted microscope, equipped with a green fluorescent filter (excitation wavelength: 450−490 nm, and emission wavelength: 500−700 mn), DAPI filter (excitation wavelength: 365 nm and emission wavelength: 445/450 nm), red filter (excitation wavelength: 407, 510, 565 nm and emission wavelength: 468, 537, 604 nm), monochromatic RGB CoolLed light source (Andover, U.K.), and monochromatic Carl Zeiss AxioCam Icm1

dx.doi.org/10.1021/ic402469t | *Inorg. Chem.* 2014, 53, 1009−1020

Scheme 1. Synthesis of the Novel Diacetylpyridine Ligands 4a−4e with Varying Aliphatic Chain Length

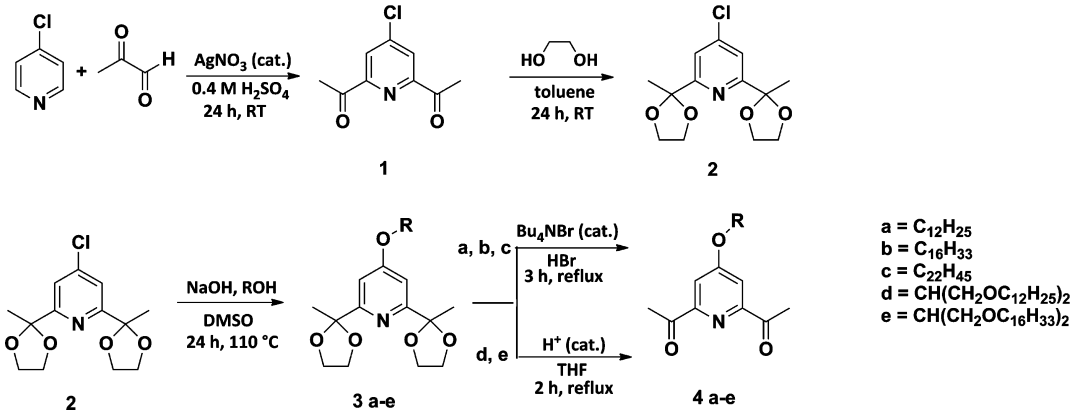

Scheme 2. Reaction Scheme for the Template Synthesis of [Mn(L1−L5)Cl$_2$]

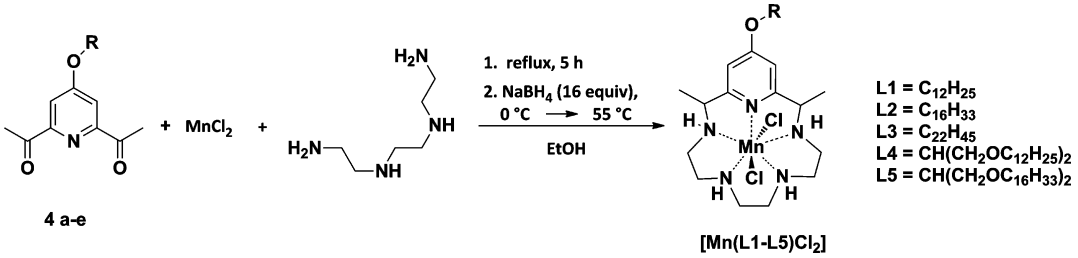

camera. All experiments were performed in triplicate. Images were postprocessed in ImageJ software (NIH, USA) where semiquantitative fluorescence intensity was determined.

Detection of Cytosolic Superoxide Level. For the semiquantification of the intracellular SOD activy of the complexes, immunostimulated RAW 264.7 macrophages were used. The murine macrophage RAW 264.7 (American Type Culture Collection) cell line was cultured at 37 °C under 5% CO_2 atmosphere in Dulbecco's modified Eagle's medium (DMEM) containing 1.0 g/L D-glucose and sodium pyruvate (Invitrogen). The medium was supplemented with 10% fetal bovine serum (Invitrogen) and penicillin/streptomycin (100 U/1 mg; Sigma Aldrich). The macrophage were stimulated with IFN-γ (20 units/mL) and LPS (50 ng/mL) to produce superoxide. Twenty-two hours after immunostimulation, cells were treated with 1, 10, and 100 μM complexes for 1.5 h and then loaded with 10 μM hydroethydine (HE) for 30 min.

Detection of Mitochondrial Superoxide Level. Hela cells were grown in DMEM medium supplemented with 10% FCS, 2 mM L-glutamine, 1% nonessential amino, and 1% penicillin-streptomycin acid at 37 °C under a 5% CO_2. Cells were treated with 1 μM and 10 μM Mn(Me$_2$-Pyane), Mn**L1**, and Mn**L2** for 90 min. After the treatment, cells were loaded with 2.5 μM MitoSox Red (Invitrogen, USA) for 20 min in Hank's Balanced Salt Solution (HBBS).

Lipid Peroxidation Assay. For the lipid peroxidation assay,[32] Raji cells were grown in RPMI 1640 medium supplemented with 10% FCS, 2 mM L-glutamine, 1% nonessential amino acid, and 1% penicillin−streptomycin at 37 °C and 5% CO_2. A total of 4.5 × 10^5 cells per sample were incubated with 10 μM Mn(Me$_2$-Pyane), Mn**L1**, and Mn**L2** for 90 min, washed two times, and placed in fresh medium supplemented with 100 μM Paraquat (PQ) overnight. The quantification of malondialdehyde (MDA) was done using a commercial fluorometric MDA assay kit according to the manufacturer's recommendations (Cayman, USA).

RESULTS AND DISCUSSION

Syntheses. The targeted manganese(II) complexes Mn**L1**−Mn**L5** with aliphatic chains of variable length and number are derivates of the SOD-active complex Mn(Me$_2$-Pyane).[33] The first synthetic step was the acetylation of 4-chloropyridine according to a method described elsewhere[23,24] that resulted in compound **1** (see Experimental Section) in a moderate yield. In order to protect the electron deficient carbon atoms of the introduced carbonyl groups from nucleophilic substitution, the diketal **2** was synthesized using a known literature method.[25] The crucial step of the synthetic procedure was to form new compounds, the 4-alkoxypyridines **3a**−**3e** (Scheme 1). It required harsh reaction conditions, i.e., an excess of NaOH and high temperatures in aprotic DMSO to substitute the chloro group in **2** with the respective alkoxide. This was achieved using a modified literature method.[26] The obtained compounds were purified by column chromatography. The representative ^{1}H NMR and ^{13}C NMR spectra are shown for compounds **3b** (Figure S1) and **3e** (Figure S2). (The NMR spectra of **3a**−**3e** only differ in intensity of the proton signals (^{1}H NMR) or number of carbon signals (^{13}C NMR) in the high field region due to an increased length of the hydrocarbon chains.) Several test reactions have proven that even the crude material, i.e., unpurified **3a**−**3e**, can be utilized for the subsequent synthetic step without losing the purity of **4a**−**4e**. The acid hydrolysis of the acetal groups in **3a**−**3e** gave rise to new compounds, the 4-alkoxy-2,6-diacetylpyridines **4a**−**4e** (Scheme 1). The representative ^{1}H and ^{13}C NMR spectra are only given for **4b** (Figure S3) and **4e** (Figure S4) in the Supporting Information. Compounds **4a**−**4e** are the direct ligand precursors. Mn**L1**−Mn**L5** were obtained using the template synthesis and a subsequent *in situ* reduction of the Schiff-base intermediates with an excess of sodium borohydride (Scheme 2)—a method already established in the literature for such types of manganese complexes.[29,33] Purification of the crude complexes was necessary in all cases and was achieved by column chromatography to give Mn**L1**−Mn**L5** in moderate yields.

dx.doi.org/10.1021/ic402469t | Inorg. Chem. 2014, 53, 1009−1020

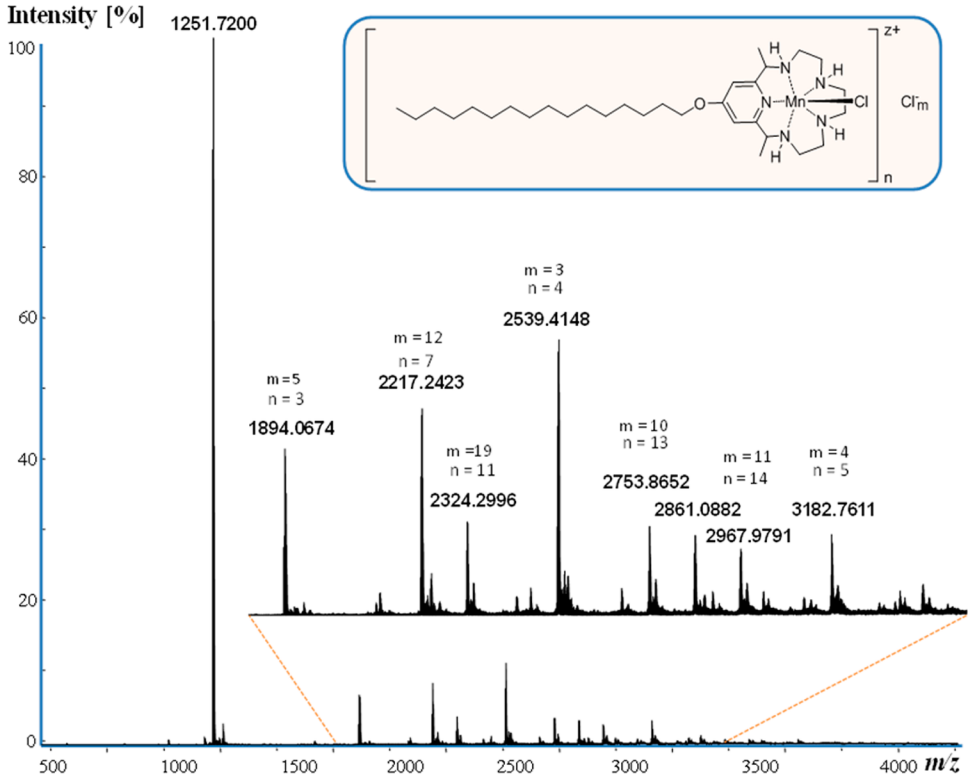

Figure 1. UHR-ESI-MS spectrum of Mn**L2** in a 1:1 MeOH/water mixture at −30 °C, showing different aggregates with varying number (n) of the {[Mn**L2**]Cl} units; [Mn**L2**] = 1×10^{-4} M; m is the number of Cl^- counteranions.

UHR-ESI-MS Measurements. In order to characterize the obtained Mn**L1**−Mn**L5** complexes in solution, UHR-ESI mass spectrometry was performed on samples of a low concentration (~1×10^{-4} M) of Mn**L1**−Mn**L3** in water and of Mn**L4** and Mn**L5** in MeOH. Even the relatively low concentrations required for mass spectrometry could not be achieved in water for Mn**L4** and Mn**L5**. A complete overview of the main species observed during the measurements is given in Table S1. The obtained spectra (Figures S5−S9) show that in the case of all complexes the main species is the intact monomeric form of the respective manganese compound ($\{[MnL]Cl\}^+$ or $[MnL]^{2+}$). In the case of complexes with **L1**−**L4**, some aggregates of two complex units $\{[MnL]_2Cl_3\}^+$, most probably formed through a bridging by the chloride anion, appear as the second prominent species.

Since interactions between the units forming supramolecular assemblies in solutions are generally weak, cryo mass spectrometry was used to exclude the possibility of aggregate destruction by high temperatures (energy) under the experimental conditions of standard MS spectrometry. MS spectra obtained at 4 °C in aqueous solution have not shown any difference in comparison to those obtained by standard measurements regarding aggregate formation. Therefore, measurements at cryogenic temperatures (i.e., −30 °C) were performed in a 1:1 MeOH/water solution of Mn**L2**, as a representative of this class of Mn complexes (Figure 1). At the applied cryogenic temperature, Mn**L2** showed quite a different behavior compared to the standard measurements (Figure S6), where the formation of charged aggregates could be observed consisting of a different number of the {Mn**L2**Cl} subunits and chloride counteranions (Figure 1). Species identified within the experimental measurements are listed in Table 1 and give a comparative overview of a size and charge of the observed aggregates, as well as their mass accuracy. Some peaks depicted in Figure 1 result from overlapping of the isotopic envelopes of differently charged aggregates with similar m/z values. An example of such highly complex isotopic patterns is illustrated in Figure S10. Assemblies of up to 15 {[Mn**L2**]Cl} units can be detected, with masses of nearly 10 000. By way of comparison, the nonsubstituted Mn(Me_2-Pyane) complex does not show any aggregation under the same experimental conditions of MS measurements (Figure S11). Thus, the supramolecular aggregation of this kind of novel Mn(II) pentaazamacrocyclic

Table 1. UHR-ESI-MS Data for MnL2 Recorded in a 1:1 MeOH/Water Mixture at −30 °C[a]

recorded m/z	calculated m/z	peak assignment
1251.7200	1251.7235	$\{[MnL2]Cl_3\}^+$
1894.0674	1894.0712	$\{[MnL2]_3Cl_5\}^+$
2217.2423	2217.2473	$\{[MnL2]_7Cl_{12}\}^{2+}$
2324.2996	2324.3053	$\{[MnL2]_{11}Cl_{19}\}^{3+}$
2538.7473	2538.7545	$\{[MnL2Cl]_{12}Cl_9\}^{3+}$
2538.9153	2538.9211	$\{[MnL2Cl]_8Cl_6\}^{2+}$
2539.4148	2539.4192	$\{[MnL2Cl]_4Cl_3\}^+$
2753.8652	2753.8700	$\{[MnL2Cl]_{13}Cl_{10}\}^{3+}$
2860.5887	2860.5949	$\{[MnL2Cl]_9Cl_7\}^{2+}$
2967.9791	2967.9860	$\{[MnL2Cl]_{14}Cl_{11}\}^{3+}$
3182.7611	3182.7698	$\{[MnL2Cl]_5Cl_4\}^+$
3183.0886	3183.1015	$\{[MnL2Cl]_{15}Cl_{12}\}^{3+}$
3183.2612	3183.2681	$\{[MnL2Cl]_{10}Cl_8\}^{2+}$

[a]Main species (with an absolute intensity ≥ 5%) representing aggregates of Mn**L2** with varying size and charge are listed. The recorded and simulated masses of the peak with the highest intensity are compared for each species.

dx.doi.org/10.1021/ic402469t | Inorg. Chem. 2014, 53, 1009−1020

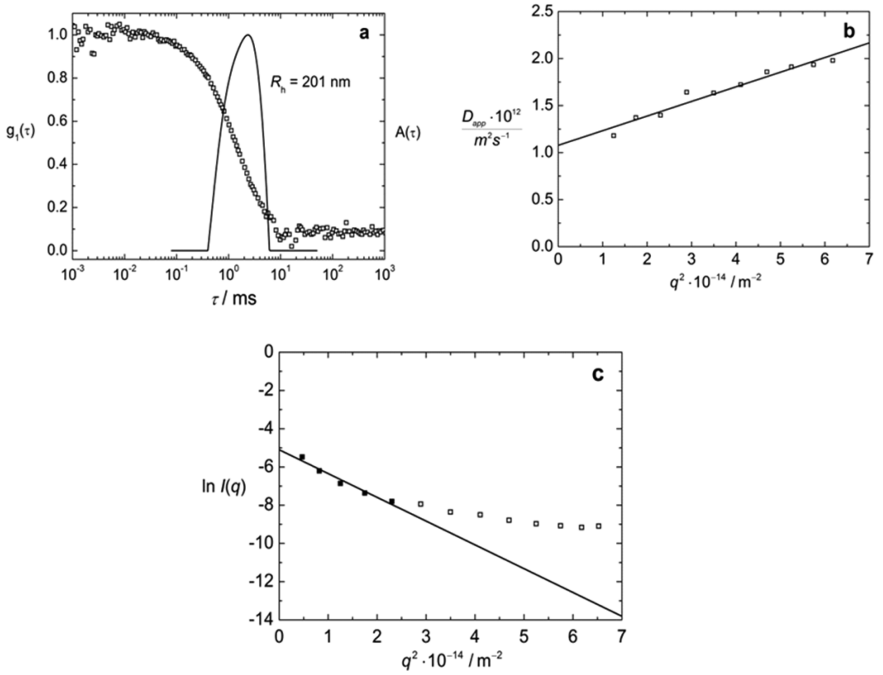

Figure 2. Dynamic and static light scattering of Mn**L1**. (a) Electric field autocorrelation function $g_1(\tau)$ and distribution of relaxation times $A(\tau)$. (b) Extrapolation of apparent diffusion coefficient to $q = 0$. (c) Static light scattering with Guinier plot for small q.

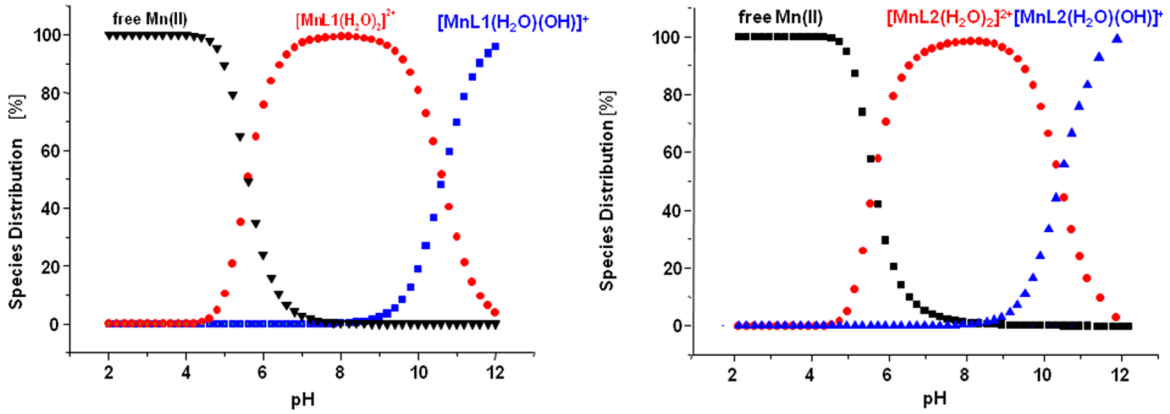

Figure 3. Species distribution for the complex Mn**L1** (left) and Mn**L2** (right) as a function of pH at 21 °C. Conditions: [complex] = 1 mM, electrolyte was 0.1 M Me_4NCl.

compound is related to their amphiphilic nature, i.e., their elongated and highly lipohilic hydrocarbon chains.

Dynamic and Static Light Scattering. Another observation regarding the water-soluble amphiphilic complexes presented in this work (Mn**L1**−Mn**L3**) is that they form tight white foam when sufficiently agitated in solution. For a better illustration of this expected effect, a comparison of three different solutions with a concentration of 1 mM containing Mn(Me_2-Pyane), Mn**L2**, or SDS is given in Figure S12. This property additionally points toward the formation of supramolecular assemblies of these complexes in aqueous solutions, which we further examined by light scattering measurements. Dynamic light scattering results for Mn**L1** are displayed in Figure 2 that show the electric field autocorrelation function and the corresponding distribution of relaxation times (Figure 2a) as well as the angular dependence of the apparent diffusion coefficient (Figure 2b). Dynamic light scattering shows that micellar aggregates with an average hydrodynamic radius of R_h = 201 nm are present in solution. The size distribution shows a standard deviation of $\sigma = 0.50$. Interestingly, with the given size distribution, despite the large aggregate size relative to the building block, there is only this one type of micellar assembly. A size of 400 nm clearly is far too large to represent a simple spherical micelle. Hence, it may be that either vesicles or cylindrical micelles have been formed. Due to the large size relative to the light scattering q range, a radius of gyration as extracted from a Guinier plot of the static light scattering data can only be considered as a rough estimate (Figure 2c). However, it results in a radius of gyration of R_g = 193 nm and a corresponding characteristic ratio of R_g/R_h = 0.96. This is consistent with the micellar aggregates having the structure of vesicles; i.e., it may be that vesicles have been formed, although the formation of cylindrical wormlike micelles cannot clearly be excluded.

Potentiometric Titrations. Due to the long and carbon-rich aliphatic chains at the pyridine moiety of the complexes Mn**L1**−Mn**L5**, the solubility of all compounds in aqueous (and more general in polar) solutions is limited. Only for

dx.doi.org/10.1021/ic402469t | Inorg. Chem. 2014, 53, 1009−1020

compounds Mn**L1** and Mn**L2** could a concentration (i.e., ≥ 1 mM) sufficient for a potentiometric titration be achieved and their protolytic equilibria be studied, resulting in a similar acid–base behavior (Figure 3). Mn**L3** was soluble in aqueous media in concentrations up to 0.5 mM, but the obtained data did not result in reasonable pK_a values or stability constants, probably due to the aggregation of Mn**L3** during the titration process.

No significant influence of the increased number of carbon atoms in the aliphatic side chains on the acid–base properties of the complexes is observed, consistent with the fact that the increased length of the carbon chain does not affect the electron density within the pyridine moiety, as confirmed by the ^{13}C NMR spectra of **4a**–**4e** and manganese centered redox potentials (vide infra).

The coordinated water ligand is just slightly more acidic in the case of Mn**L1** and Mn**L2** (*ca.* pK_{H_2O} = 10.6) compared to Mn(Me$_2$-Pyane) that shows pK_{H_2O} = 10.96. This can be attributed to the electron withdrawing ability of the oxygen atom of the ether functionality adjacent to the pyridine moiety that slightly influences the electron density on the metal center in Mn**L1** and Mn**L2**. The species distribution shows that over a broad pH range (pH 5.5–11.0 for Mn**L1** and pH 6.5–11.2 for Mn**L2**) the diaqua-complex is the predominant form for both compounds (Figure 3). According to the potentiometric data the amphiphilic complexes do not form stable protonated forms $[Mn(\mathbf{L} + H^+)(H_2O)_2]^{3+}$ (log K_{MHL} of 3.00 and 2.42 for $[Mn(\mathbf{L1} + H^+)]^{3+}$ and $[Mn(\mathbf{L2} + H^+)]^{3+}$, respectively), which is in contrast to Mn(Me$_2$-Pyane) and other known seven-coordinate Mn(II) complexes, where a thermodynamic stability of protonated forms is significant.[10,33,34]

Consequently, a decrease of pH results in the dechelation and release of manganese in the solution, which is illustrated by the pMn values under corresponding conditions. As can be seen in Table 2, the amount of free Mn(II) at given pH increases by the following trend: Mn(Me$_2$-Pyane) < Mn**L1** < Mn**L2**. Thus, the thermodynamic stability constant of the complexes Mn**L1** and Mn**L2**, expressed by log K_{ML}, is considerably lower when compared to that of Mn(Me$_2$-Pyane) (Table 2).

Table 2. pMn Values, Stability Constants, and p*K* Values for MnL1, MnL2, Mn(Me$_2$-Pyane), and Corresponding Ligands Determined by Potentiometric Titration at 21 °C, [Complex] = 1 mM

	MnL1	MnL2	Mn(Me$_2$-Pyane)[a]
pK_1[b]	3.00	2.43	5.24
pK_2[b]	10.43	6.57	9.35
pK_3[b]	n.d.	n.d.	9.96
pK_{H2O}	10.61	10.63	10.96
log K_{MHL}[c]	2.43	1.59	5.66
log K_{ML}[d]	9.74	9.26	11.25
pMn (pH 7.4)[e]	4.36	3.99	4.90
pMn (pH 8.1)[e]	5.24	4.62	5.65

[a]Ref 33. [b]Ligand pK_a values related to the (de)protonation of the secondary ammine groups of free ligands, i.e., pK_1 = $[LH_2^{2+}][H^+]/[LH_3^{3+}]$, p$K_2$ = $[LH^+][H^+]/[LH_2^{2+}]$, and pK_3 = $[L][H^+]/[LH^+]$. [c]K_{MHL} = [MHL]/[ML][H], related to the protonation of one of the secondary ammine groups in the complexes. [d]K_{ML} = [ML]/[M][L]. [e]pMn = $-\log[Mn(II)]_{free}$ calculated for [complex] = 1 mM and T = 21 °C.

Electrochemistry. Metal centered redox potentials of Mn**L1**–Mn**L5** have been determined in MeOH and DMSO (Table 3). The cyclic voltammograms (CVs) of Mn**L1**–Mn**L5** show a similar behavior to that already observed in the literature for pentaazamacrocyclic Mn(II) complexes.[10,34] Electrochemical studies of Mn**L4** and Mn**L5** could not be performed in MeOH due to solubility problems.

Table 3. Redox Potentials $E_{1/2}$ (Mn(II)/Mn(III)) of MnL1–MnL5 in DMSO and MeOH vs SHE, [Complex] = 1 mM, T = 21 °C

compound	$E_{1/2}$ vs SHE (DMSO)	ΔE[a]	$E_{1/2}$ vs SHE (MeOH)	ΔE[a]
Mn**L1**	0.87 V	112 mV	0.98 V	132 mV
Mn**L2**	0.83 V	99 mV	0.97 V	122 mV
Mn**L3**	0.90 V	106 mV	0.97 V	129 mV
Mn**L4**	0.86 V	176 mV		
Mn**L5**	0.88 V	70 mV		
Mn(Me$_2$-Pyane)[b]	0.87 V	140 mV	0.95 V	130 mV
M40403	0.94 V	133 mV	0.84 V	100 mV

[a]Scan rate 0.10 V s^{-1}. [b]Ref 35.

The hydrocarbon chains in the *para* position to the pyridine nitrogen do not significantly influence the redox behavior of the compounds when compared to the model complex Mn(Me$_2$-Pyane).[10] In general, the observed high positive redox potentials in such media (Table 3) indicate a relatively high thermodynamic stability of the Mn(II) forms of Mn**L1**–Mn**L3** against air oxidation and are in good agreement with the redox potentials reported for similar compounds.[10,34] Exemplary CVs of Mn**L1** in MeOH and DMSO are represented in Figure 4. More positive $E_{1/2}$ values are observed in MeOH (Table 3, Figures 4 and S13) as a protic solvent that stabilizes the Mn(II) state even more.

The peak separation in the CVs of Mn**L1**, Mn**L2**, Mn**L3**, and Mn**L5** demonstrates their quasi-reversible Mn(II)/Mn(III) redox-behavior in the applied organic solvents (Figure S13). Mn**L4** shows an irreversible electrochemical behavior, with ΔE = 176 mV, which may be a consequence of some aggregation and/or a deposition on the electrode surface (the overall quality of the CV is poor, due to a low current). The peak separation in MeOH is larger than in DMSO, suggesting a somewhat different speciation in these two solvents. It may be the consequence of a different level of aggregation in these two solvents. In addition, protolytic equilibria (Mn-OMe/Mn-MeOH)[36] may play a role in the MeOH solution.

SOD-Activity Determined by Stopped-Flow Measurements. The SOD-activity of Mn**L1**–Mn**L3** was tested *in vitro* with a rapid scan stopped-flow technique.[21] Mn**L4** and Mn**L5** could not be tested due to the limited solubility in aqueous media (*vide supra*). The obtained catalytic rate constants are listed in Table 4 and are compared with the SOD activity of the unsubstituted compound Mn(Me$_2$-Pyane).[21] The SOD mimetics with elongated aliphatic hydrocarbon chains, Mn**L1**, Mn**L2**, and Mn**L3**, experience a drop in the SOD activity *in vitro* at pH 7.4 in comparison to Mn(Me$_2$-Pyane), in both the presence and absence of phosphate. In the absence of phosphate (in the HEPES buffer), a decrease in k_{cat} of nearly 50% for Mn**L1**–Mn**L3** compared to Mn(Me$_2$-Pyane) at pH 7.4 (Table 4, Figure S14) is observed, which might be related to the formation of supramolecular aggregates. As a consequence,

dx.doi.org/10.1021/ic402469t | *Inorg. Chem.* 2014, 53, 1009–1020

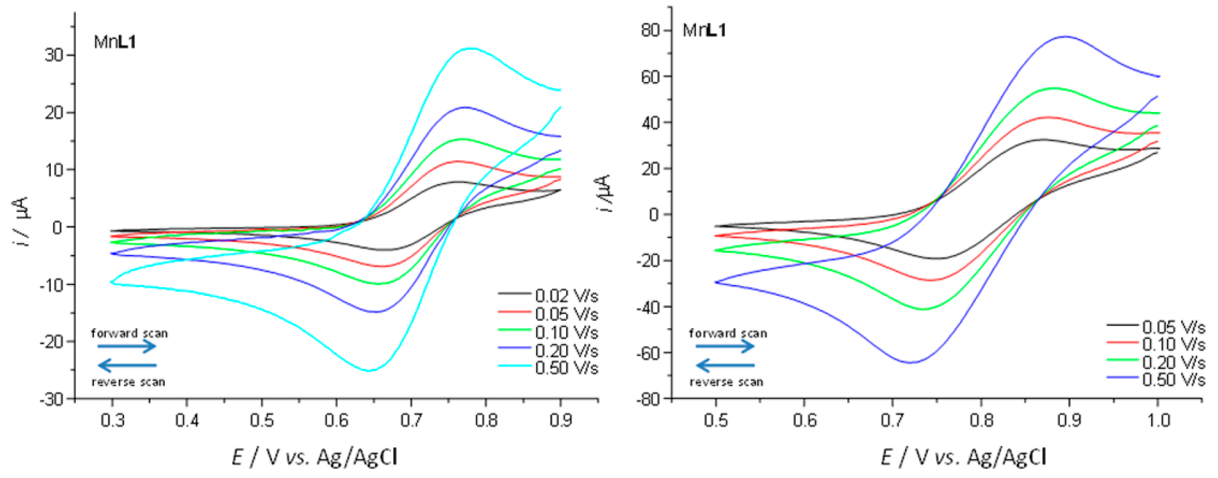

Figure 4. Cyclic voltammograms of 1 mM Mn**L1** in DMSO (left) and MeOH (right) with varying scan rates (0.1 M Bu_4NPF_6 in DMSO and $LiClO_4$ in MeOH, respectively, as supporting electrolytes).

Table 4. Second Order Rate Constants k_{cat} at 21 °C for Catalytic Dismutation of Superoxide with MnL1−MnL3, Mn(Me$_2$-Pyane), and for Uncatalyzed Superoxide Dismutation

compound	HEPES pH 7.4[a] k_{cat} [× 10^6 M^{-1} s^{-1}]	HEPES pH 8.1[a] k_{cat} [× 10^6 M^{-1} s^{-1}]	phosphate pH 7.4[b] k_{cat} [× 10^6 M^{-1} s^{-1}]
Mn**L1**	14.3 ± 1.8	12.3 ± 0.2	5.90 ± 0.3
Mn**L2**	15.1 ± 2.1	12.1 ± 0.5	2.90 ± 0.1
Mn**L3**	14.1 ± 0.1	12.2 ± 0.2	1.40 ± 0.1
Mn(Me$_2$-Pyane)[c]	27.3 ± 0.4	12.1 ± 0.2	8.40 ± 0.2
uncatalyzed[c,d]	~0.5	0.13 ± 0.01	0.51 ± 0.01

[a]60 mM. [b]50 mM. [c]Ref 21. [d]Ref 10.

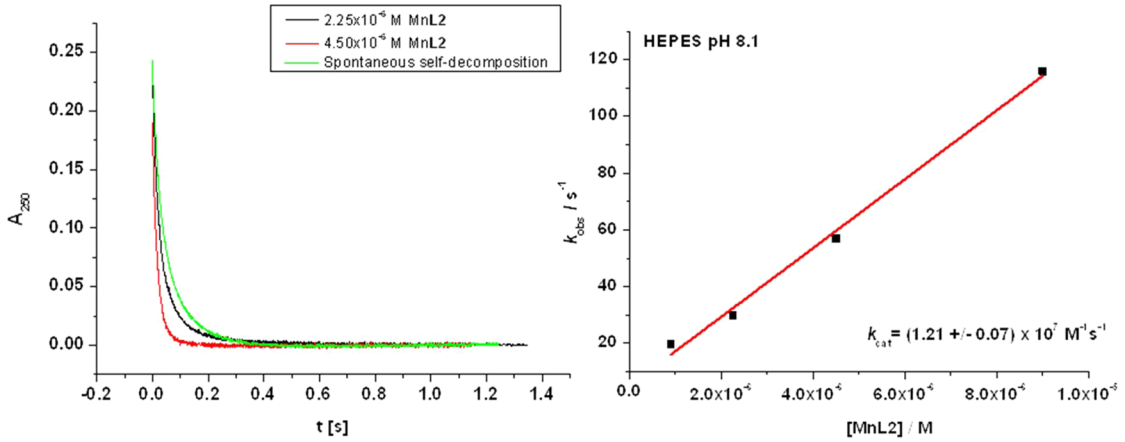

Figure 5. Left: Kinetic traces (at 250 nm) for the self-decomposition of $O_2^{\bullet-}$ and catalyzed by Mn**L2**. Right: Plot of k_{obs} versus [Mn**L2**] for decomposition of superoxide (2.0×10^{-4} M superoxide in DMSO was mixed with Mn**L2** in 60 mM HEPES buffer, pH 8.1 at 21 °C, in a 1/10 volume ratio).

some of the active centers within these assemblies are probably less accessible for superoxide from the bulk polar medium. On the other hand, the long aliphatic chain on the macrocycle could increase an activation barrier required for the ligand conformational change upon the superoxide binding and/or formation of a Mn(III) intermediate species (with or without bound peroxide) that prefers a six-coordinate geometry.[37,38] This would slow down the catalytic rate independent of the aggregation.

The presence of large amounts of phosphate (50 mM buffer solution) is in general responsible for a decrease in SOD activity for all macrocyclic polyamine Mn(II)-SODm tested *in vitro* so far.[10,21] This drop ranges from 2.4 times for Mn**L1** up to 10 times for Mn**L3** (Table 4, Figure S14). A trend in k_{cat} at pH 7.4 in a phosphate buffer (Mn(Me$_2$-Pyane) > Mn**L1** > Mn**L2** > Mn**L3**) seems to follow the trend in complex thermodynamic stability (Table 3). Though log K_{ML} was not determined for Mn**L3**, it can be assumed that an increase in the length of the aliphatic chain causes a decrease in the complex stability, as observed for Mn**L1** and Mn**L2**. However, it has been previously shown that phosphate tends to coordinate to the active center of such types of SODm and can consequently inactivate them toward superoxide binding.[21] It was recently shown that in the case of M40403, which belongs to the same family of MnSOD mimetics with two cyclohexane moieties, the presence of phosphate induces even a 25-fold decrease of its

dx.doi.org/10.1021/ic402469t | *Inorg. Chem.* 2014, 53, 1009−1020

SOD activity.[21] Importantly, these and other literature studies[34,35] have shown that phosphate does not contribute to the complex decomposition, i.e., manganese dechelation, and that the decrease in SOD activity is not related to complex instability but to phosphate-specific interactions with the complex that are of electrostatic or coordinative nature.[21] By way of comparison, k_{cat}'s observed from M40403 ($0.19 \pm 0.01 \times 10^7$ M^{-1} s^{-1}) and Mn**L3** ($0.14 \pm 0.01 \times 10^7$ M^{-1} s^{-1}) under the same experimental conditions, in the presence of phosphate, are almost identical. Our MS studies also do not show any significant decomposition (i.e., only a minor amount of free ligand) of the amphiphilic Mn**L1**−Mn**L3** complexes caused by the presence of phosphate as exemplified by a mass spectrum of Mn**L2** in the presence of a 10-fold excess of phosphate species (Figure S15). It can be just speculated that the interaction with phosphate becomes more prominent following the Mn(Me_2-Pyane) < Mn**L1** < MnL2 < Mn**L3** order.

On the other hand, under slightly basic conditions at pH 8.1 (related to the mitochondrial milieu), the SOD activity of the hydrocarbon-rich Mn**L1**−Mn**L3** SOD mimetics (Figure 5 and Figure S16) is identical with that of Mn(Me_2-Pyane) (Table 4). Even more, M40403 (which passed phase II clinical trials)[39] has the same $k_{cat} = 1.24 \pm 0.07 \times 10^7$ M^{-1} s^{-1} under the corresponding experimental conditions.[21]

Cell Culture Studies. In order to compare the effects of the studied SOD mimics on the superoxide levels in the cytosol, we treated immunostimulated RAW264.7 macrophages with various concentrations of Mn**L1**, Mn**L2**, and Mn(Me_2-Pyane) and then measured their ability to remove superoxide and prevent the oxidation of hydroethydine (cytosolic fluorescent sensor for superoxide). Cells were treated with the complexes 22 h after the immunostimulation was started, at the time when production of superoxide reaches its maximum.[40] All experiments were performed in triplicate, and the data analysis was performed on at least 100 cells.

As shown in Figure 6, Mn**L1** exhibits a significant effect already at 1 μM concentration, with 10 μM being even more efficient. A 100 μM concentration was, however, toxic (with a certain percentage of the cells being dead, not shown) and an increase of the fluorescence signal was observed if compared to the other two concentrations. Mn**L2** had an even more pronounced effect at a 1 μM concentration, but the 100 μM complex led to cell detachment and death. Mn(Me_2-Pyane) had a more moderate effect, with mild superoxide scavenging at low concentrations (1 and 10 μM), but a somewhat stronger effect was observed in cells treated with a 100 μM complex. When compared (Figure 6), the effect of 100 μM Mn(Me_2-Pyane) matches that of 10 μM Mn**L1** and 1 μM Mn**L2**. Although the used methodology is more at a qualitative level,[41] the observed trends clearly show the differences in reduction of oxidative stress caused by studied complexes.

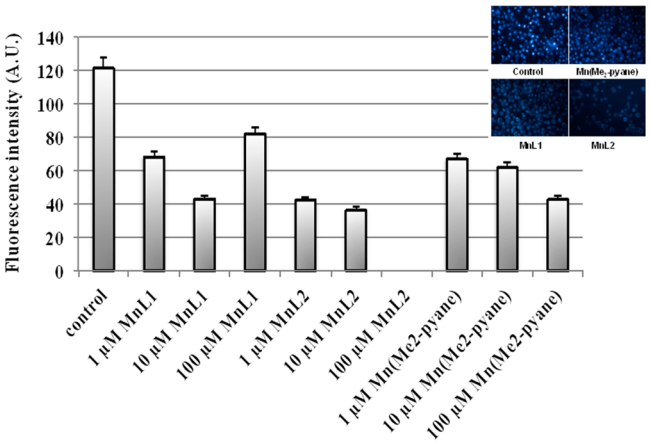

Figure 6. The effect of SOD mimics on intracellular superoxide levels, measured with fluorescent dye hydroethidine. All experiments were performed in triplicate. The values represent the mean fluorescence of at least 100 cells ± SEM. Inset: Original photomicrographs of RAW 264.7 cells after 1.5 h incubation without or with 10 μM Mn(Me_2-Pyane), Mn**L1**, and Mn**L2**, artificially colored blue.

The experiments on HeLa cells have also suggested that Mn**L1** and Mn**L2**, in comparison to Mn(Me_2-Pyane), exhibit higher efficiency in decreasing the basal mitochondrial level of superoxide (Figure 7). It should be mentioned that at a pH of around 8, which is related to mitochondria's slightly alkaline environment, all three complexes exhibit the same SOD activity *in vitro* (Table 4). Thus, the observed differences may be related to the higher lipophilicity of Mn**L1** and Mn**L2** that generally supports easier penetration through the cell membranes. Consequently, Mn**L1** and Mn**L2** may much faster reach the active concentration required for the efficient superoxide removal within the cell, while for the same incubation time, higher doses are needed for Mn(Me_2-Pyane), whose diffusion through the lipid bilayer is slower.

Furthermore, we have tested the effect of 10 μM Mn(Me_2-Pyane), Mn**L1**, and Mn**L2** on the prevention of the lipid peroxidation induced by paraquat *via* its superoxide generation. (The chosen 10 μM concentration was proven to be quite effective in decreasing a cytosolic superoxide level in the case of both Mn**L1** and Mn**L2**, Figure 6.) Upon treatment with Mn**L1**, the lipid peroxidation drops to a basal level, whereas treatment with Mn**L2** causes its decline even below a basal level. As demonstrated in Figure 8, the inhibition of the induced lipid peroxidation by studied complexes follows the Mn(Me_2-Pyane) < Mn**L1** < Mn**L2** order. The obtained results are in agreement with the general ability of these complexes to decrease the superoxide level within both cytosol and mitochondria and might also reflect the trend in the increased complex lipophilicity and consequently an increased accumulation in the lipids. Although the higher lipophilicity increases the affinity of the complexes toward lipid cell compartments and the higher activity would be expected only locally, around the membranes, we cannot exclude endocytosis as a mechanism for the cellular uptake, parallel to diffusion. This would increase the overall concentration of the complex in the cytosol and contribute to the reduction of the oxidative stress observed in Figure 6.

By way of comparison, a similar effect of the complex lipophilicity on their in vivo ability to suppress oxidative stress was established for the Mn(III) N-alkylpyridylporphyrins,[42,43] which belong to another important class of SOD mimetics.[6] For example, it was reported that meta isomer MnTE-3-PyP accumulates 10-times more in *E. coli* due to a higher lipophilicity compared to the orto isomer MnTE-2-PyP, which on the other hand exhibits higher SOD activity. Consequently, MnTE-3-PyP and MnTE-2-PyP have equal efficiency to SOD-deficient *E. coli*, representing an excellent compensation scenario.[43]

■ CONCLUSION

The newly functionalized manganese pentaazamacrocyclic SOD mimetics with linear aliphatic chains exhibit the same redox

dx.doi.org/10.1021/ic402469t | Inorg. Chem. 2014, 53, 1009−1020

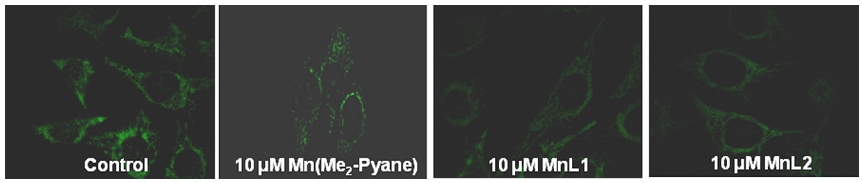

Figure 7. Suppressive effect of 10 μM Mn(Me_2-Pyane), Mn**L1**, and Mn**L2** on basal mitochondrial superoxide level in HeLa cells.

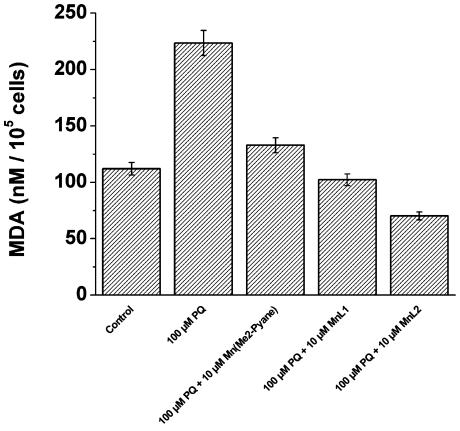

Figure 8. Quantification of malondialdehyde (MDA) upon paraquat (PQ) induced lipid peroxidation in Raji cells. Cells were treated with 10 μM Mn(Me_2-Pyane), Mn**L1**, or Mn**L2** for 90 min; washed; and incubated with 100 μM PQ overnight. (Control: basal cell level of MDA.)

properties (in MeOH and DMSO) and SOD activity at pH = 8.1 (in a HEPES buffer) as the nonsubstituted Mn(Me_2-Pyane) analogue. In general, they show a somewhat lower thermodynamic stability, which decreases with the elongation of the hydrocarbon chain. The cryo-mass spectrometry, performed on the selected compound, indicated the formation of supramolecular aggregates, and the light scattering has demonstrated the existence of predominantly one type of micellar assembly, with an average 400 nm size. The amphiphilic complexes exhibit lower SOD activity at pH 7.4 in comparison to that of the nonsubstituted complex, in particular in the presence of phosphate. Despite these in vitro results, cell culture studies of the effect of the SOD mimetics on the superoxide level in the cytosol and mitochondria, as well as on the prevention of the lipid peroxidation, have clearly indicated that increased lipophilicity enhances the beneficial biological effects of this type of complex at low concentrations. This is most probably a result of the improved diffusion through the lipid bilayer of the cell membranes enhanced by the increase in the complex lipophilicity. However, at concentrations higher than ca. 10 μM, toxic effects have been observed that become more prominent with elongation of the aliphatic chain. Thus, further structural optimizations are required in order to diminish toxic effects, while still promoting cell uptake of these SOD mimetics.[16]

■ ASSOCIATED CONTENT

Supporting Information

Available are NMR data, stopped-flow data, electrochemical data, and mass spectra/data of relevant compounds. This material is available free of charge via the Internet at http://pubs.acs.org.

■ AUTHOR INFORMATION

Corresponding Author

*Tel.: +49 9131 8525428. Fax: +49 9131 8527345. E-mail: ivana.ivanovic@chemie.uni-erlangen.de.

Notes

The authors declare no competing financial interest.

■ ACKNOWLEDGMENTS

Financial support by the intramural grant from the Friedrich-Alexander University of Erlangen−Nürnberg (Emerging Field Initiative: Medicinal Redox Inorganic Chemistry) is gratefully acknowledged. The authors also thank Oliver Tröppner for recording the ESI-mass spectra.

■ REFERENCES

(1) Evbuomwan, O. M.; Kiefer, G.; Sherry, A. D. *Eur. J. Inorg. Chem.* **2012**, *12*, 2126−2134.
(2) Kielar, F.; Tei, L.; Terreno, E.; Botta, M. *J. Am. Chem. Soc.* **2010**, *132*, 7836−7837.
(3) Espinet, P.; García-Orodea, E.; Miguel, J. A. *Inorg. Chem.* **2000**, *39*, 3645−3651.
(4) Román-Martínez, M. C.; Diáz-Aunión, J. A. *Catal. Lett.* **2001**, *77*, 41−46.
(5) (a) Riley, D. P. *Chem. Rev.* **1999**, *99*, 2573−2587. (b) Muscoli, C.; Cuzzocrea, S.; Riley, D. P.; Zweier, J. L.; Thiemermann, C.; Wang, Z.-Q.; Salvemini, D. *Br. J. Pharmacol.* **2003**, *140*, 445−460. (c) Iranzo, O. *Bioorg. Chem.* **2011**, *39*, 73−87.
(6) (a) Batinić-Haberle, I.; Rebouças, J. S.; Spasojević, I. *Antioxid. Redox Signaling* **2010**, *13*, 877−918. (b) Tovmasyan, A.; Spasojevic, I. *BioInorg. React. Mech.* **2013**, *9* (1−4), DOI: 10.1515/irm-2013-0004.
(7) Drahos, B.; Lukes, I.; Toth, E. *Eur. J. Inorg. Chem.* **2012**, *12*, 1975−1986.
(8) Pan, D.; Caruthers, S. D.; Senpan, A.; Schmieder, A. H.; Wickline, S. A.; Gregory, M. L. *Nanomed. Nanobiol.* **2011**, *3*, 162−173.
(9) Kueny-Stotz, M.; Garofalo, A.; Felder-Flesch, D. *Eur. J. Inorg. Chem.* **2012**, *12*, 1987−2005.
(10) Lieb, D.; Friedel, F. C.; Yawer, M.; Zahl, A.; Khusniyarov, M. M.; Heinemann, F. W.; Ivanović-Burmazović, I. *Inorg. Chem.* **2013**, *52*, 222−236.
(11) Laurent, S.; Henoumont, C.; Vander Elst, L.; Muller, R. N. *Eur. J. Inorg. Chem.* **2012**, *12*, 1889−1915.
(12) Lavasanifar, A.; Samuel, J.; Kwon, G. S. *Adv. Drug Delivery Rev.* **2002**, *54*, 169−190.
(13) Accardo, A.; Tesauro, D.; Aloj, L.; Pedone, C.; Morelli, G. *Coord. Chem. Rev.* **2009**, *253*, 2193−2213.
(14) Andre, J. P.; Toth, E.; Fischer, H.; Seelig, A.; Macke, H. R.; Merbach, A. E. *Chem.—Eur. J.* **1999**, *5*, 2977−2983.
(15) (a) Kenzler, T. W.; Trush, M. A. *Biochem. Pharmacol.* **1983**, *32*, 3485−3487. (b) Kenzler, T. W.; Bush, D. M.; Kozumbo, W. J. *Science* **1983**, *221*, 75−77.
(16) Rajic, Z.; Tovmasyan, A.; Spasojevic, I.; Sheng, H.; Lu, M.; Li, A. M.; Gralla, E. B.; Warner, D. S.; Benov, L.; Batinić-Haberle, I. *Free Radical Biol. Med.* **2012**, *52*, 1828−1834.
(17) Kelso, G. F.; Maroz, A.; Cochemé, H. M.; Logan, A.; Prime, T. A.; Peskin, A. V.; Winterbourn, C. C.; James, A. M.; Ross, M. F; Brooker, S.; Porteous, C. M.; Anderson, R. F.; Murphy, M. P.; Smith, R. A. J. *Chem. Biol.* **2012**, *19*, 1237−1246.

(18) (a) Salvemini, D.; Wang, Z.-Q.; Zweier, J. L.; Samouilov, A.; Macarthur, H.; Misko, T. P.; Currie, M. G.; Cuzzocrea, S.; Sikorski, J. A.; Riley, D. P. *Science* **1999**, *286*, 304−306. (b) Riley, D. P.; Schall, O. F. *Adv. Inorg. Chem.* **2007**, *59*, 233−263.
(19) (a) Filipović, M. R.; Duerr, K.; Mojović, M.; Simeunović, V.; Zimmermann, R.; Niketić, V.; Ivanović-Burmazović, I. *Angew. Chem., Int. Ed. Engl.* **2008**, *47*, 8735−8739. (b) Filipović, M. R.; Koh, A. C.; Arbault, S.; Niketić, V.; Debus, A.; Schleicher, U.; Bogdan, C.; Guille, M.; Lemaître, F.; Amatore, C.; Ivanović-Burmazović, I. *Angew. Chem., Int. Ed. Engl.* **2010**, *49*, 4228−4232. (c) Ivanović-Burmazović, I.; Filipović, M. R. Reactivity of Manganese Superoxide Dismutase Mimics toward Superoxide and Nitric Oxide: Selectivity *versus* Cross-Reactivity. In *Advances in Inorganic Chemistry*; van Eldik, R., Ed; Elsevier: Amsterdam, Netherlands, 2012; pp 53−95.
(20) Salvemini, D. Analgesic methods using synthetic catalysts for the dismutation of superoxide radicals. WO patent 98/58636, December 30, 1998.
(21) Friedel, F. C.; Lieb, D.; Ivanović-Burmazović, I. *J. Inorg. Biochem.* **2012**, *109*, 16−32.
(22) Filipović, M. R.; Koh, A. C.; Arbault, S.; Niketić, V.; Debus, A.; Schleicher, U.; Bogdan, C.; Guille, M.; Lemaître, F.; Amatore, C.; Ivanović-Burmazović, I. *Angew. Chem., Int. Ed. Engl.* **2010**, *49*, 4228−4232.
(23) Busto, E. *Adv. Synth. Catal.* **2006**, *348*, 2626−2632.
(24) Wang, C.-J.; Tu, H.-Y.; Pan, K.-H.; Zhang, A.-D. *Chem. Reagents (Beijing, China)* **2006**, *28*, 53−54.
(25) Dumont, A.; Jacques, V.; Desreux, J. F. *Tetrahedron* **2000**, *56*, 2043−2052.
(26) Katritzky, A. R.; Murugan, R. *J. Chem. Soc., Perkin Trans.* **1987**, *2*, 1867−1869.
(27) Loosli, F.; Doval, D. A.; Grassi, D.; Zaffalon, P.-L.; Favarger, F.; Zumbuchl, A. *Chem. Commun.* **2012**, *48*, 1604−1606.
(28) Espinet, P.; Garcia-Orodea, E.; Miguel, J. A. *Inorg. Chem.* **2000**, *39*, 3645−3651.
(29) Aston, K. W.; Rath, N.; Naik, A.; Slomczynska, U.; Schall, O. F.; Riley, D. P. *Inorg. Chem.* **2001**, *40*, 1779−1789.
(30) (a) Gran, G. *Analyst* **1952**, *77*, 661−671. (b) Gran, G. *Anal. Chim. Acta* **1988**, *206*, 111−123. (c) Martell, A. E.; Motekaitis, R. J. *Determination and Use of Stability Constants*; VCH: Weinheim, Germany, 1992.
(31) Zuberbühler, A. D.; Kaden, T. A. *Talanta* **1982**, *29*, 201−206.
(32) (a) Day, B. J.; Shawen, S.; Liochev, S. I.; Crapo, J. D. *J. Pharmacol. Exp.* **1995**, *275*, 1227−1232. (b) Mollace, V.; lannone, M.; Muscoli, C.; Palma, E.; Granato, T.; Rispoli, V.; Nisticò, R.; Rotiroti, D.; Salvemini, D. *Neurosci. Lett.* **2003**, *335*, 163−166.
(33) Dees, A.; Zahl, A.; Puchta, R.; van Eikema Hommes, N. J. R.; Heinemann, F. W.; Ivanović-Burmazović, I. *Inorg. Chem.* **2007**, *46*, 2459−2470.
(34) Drahoš, B.; Kotek, J.; Hermann, P.; Lukeš, I.; Tóth, E. *Inorg. Chem.* **2010**, *49*, 3224−3238.
(35) Friedel, F. C. Tuning of redox potentials of seven-coordinate iron and manganese complexes for superoxide dismutation and reaction with cytochrome c. Ph.D. Dissertation, University of Erlangen-Nürnberg, Germany, November 2012.
(36) Ivanović-Burmazović, I.; Hamza, M. S. A.; van Eldik, R. *Inorg. Chem.* **2006**, *45*, 1575−1584.
(37) Aston, K.; Rath, N.; Slomczynska, U.; Schall, O. F.; Riley, D. P. *Inorg. Chem.* **2001**, *40*, 1779−1789.
(38) Maroz, A.; Kelso, G. F.; Smith, R. A.; Ware, D. C.; Anderson, R. F. *J. Phys. Chem.* **2008**, *112*, 4929−4935.
(39) Salvemini, D.; Doyle, T. M.; Cuzzocrea, S. *Biochem. Soc. Trans.* **2006**, *34*, 965−970.
(40) Amatore, C.; Arbault, S.; Bouton, C.; Drapier, J. C.; Ghandour, H.; Koh, A. *ChemBioChem* **2008**, *9*, 1472−1480.
(41) Zhao, H.; Joseph, J.; Fales, H. M.; Sokoloski, E. A.; Levine, R. L.; Vasquez-Vivar, J.; Kalyanaraman, B. *Proc. Natl. Acad. Sci. U. S. A.* **2005**, *102*, 5727−5732.
(42) Kos, I.; Benov, L.; Spasojević, I.; Rebouças, J. S.; Batinić-Haberle, I. *J. Med. Chem.* **2009**, *52*, 7868−7872.
(43) Okado-Matsumoto, A.; Batinić-Haberle, I.; Fridovich, I. *Free Radical Biol. Med.* **2004**, *37*, 401−410.